Effect of triethanolamine on the pyrolysis of metal-propionate-based solutions

Silvia Rasi[1,2], Susagna Ricart[2], Xavier Obradors[2], Teresa Puig[2], Pere Roura-Grabulosa[1] and Jordi Farjas[1]

[1] University of Girona, Campus Montilivi, Edif. PII, E17003 Girona, Catalonia, Spain
[2] Institut de Ciència de Materials de Barcelona, ICMAB – CSIC, Campus UA Barcelona, E-08193 Bellaterra, Catalonia, Spain

*Corresponding author: Silvia Rasi (silvia.rasi@udg.edu ; srasi@icmab.es)

Abstract

The effect of triethanolamine (TEA) on single-salt propionate-based solutions used to prepare $YBa_2Cu_3O_{7-\partial}$ (YBCO) has been studied through thermal analysis, for film and powder samples. Decomposition has been followed by thermogravimetry (TG) coupled to differential scanning calorimetry (DSC) and evolved gas analysis (EGA-MS and TG-FTIR), while chemical characterization has been carried out by FTIR, XRD and EA. The addition of TEA has little effect on the decomposition of the barium salt. Conversely, the thermal behavior of the copper and yttrium propionate salt with TEA becomes more gradual and less affected by a change of atmosphere than the TEA-free case. This is explained by the fact that the decomposition mechanism is driven by the formation of an ester between the propionate groups and the TEA's OH groups, which is promoted by inert atmospheres and temperatures above 200°C. Just like the single salt precursors, the films of the barium and yttrium salts show residual organic material at 500°C in thick films decomposed in O_2.

Keywords: Triethanolamine complexes; thermogravimetric analysis; metal propionates, EGA-MS; TG-FTIR.

• Introduction

Chemical solution deposition (CSD) methods [1] of metalorganic compounds have attracted attention due to their easy accessibility and low costs when compared to physical methods used to fabricate coated conductors (CCs) [2]. CSD methods are based on the design of a solution that can be deposited on a surface to undergo two main thermal steps: pyrolysis, during which all the organic material is removed and intermediate inorganic phases are formed; and growth, at higher temperatures, during which the oxide layer crystallizes from these intermediates.

In the case of advanced oxides that involve more than one metal precursor, such as the case of superconductive tapes, one of the main challenges of CSD methods is to achieve a homogeneous distribution of all starting species by avoiding phase segregation, buckling and cracks [3] during the thermal treatments, since they

can induce low current percolation [4,5], leading to a drop in the final properties of the superconductor. Therefore, achieving good control of the final properties of the film depends on having a good control of the deposition and pyrolysis stages, since these defects arise from the shrinkage of the film during decomposition. In fact, thermal treatments are normally long in order to reduce tension and obtain stress-free films. However, time constitutes a crucial process parameter in an industrial context. Therefore, to ensure stability in the deposited layer, additives [6] such as triethanolamine (TEA) are added, since they help to reduce stress and improve rheological properties by increasing the viscosity of the initial solution.

In particular, besides being used for preparation of cosmetics, surfactants, cement and nanostructures, TEA is of special interest because of its chelating properties [7,8]. In fact, as an aminoalcohol, its properties lie between those of amines and alcohols, allowing it to act as both N-donor and O-donor thanks to the three OH groups. Therefore, while increasing viscosity, TEA is expected to form complexes and to increase the stability of the metal carboxylate salts in solution. It is known that copper can form stable complexes with nitrogen and oxygen donors [9–11]; similarly, Y^{3+} has been reported to form complexes with TEA [8], while Ba^{2+} is not expected to coordinate with TEA [12,13].

Regarding TEA thermal decomposition during pyrolysis [14,15], the aspect ratio of the sample being treated is expected to play a role [16]. When in the form of a film, TEA is likely to evaporate before reaching its decomposition temperature (250-300°C), thanks to the high surface to volume ratio. When it is placed inside a crucible, evaporation is significantly slowed down; thus, it can be heated to higher temperatures (above 300°C) where it decomposes, releasing acetaldehyde (CH_3CHO), CO_2, ammonia (NH_3) and ethylene oxide (CH_2OCH_2) [14,16]. On the other hand, metalorganic complexes of TEA are expected to decompose following several decomposition steps [17], which start with the loss of small TEA units and end with the metal salt decomposition.

Metal propionate salts have been shown to decompose following a radical path in inert atmosphere and high temperatures, releasing a symmetrical ketone (3-pentanone) and CO_2 [18–23] and forming the corresponding oxides (for yttrium propionate) or carbonates (for barium propionate) by 500°C. In O_2, oxidative degradation of the ligand is expected to occur at low temperature, releasing propionic acid, acetaldehyde, CO_2 and water, but without changing the final phases [24–26]. Conversely, for copper propionate, propionic acid is expected to be the main volatile, independently of the atmosphere [25], followed by acetaldehyde and CO_2, while the solid product is the corresponding oxide in films, and metallic copper in powders.

In this work, we will apply thermal analysis (TA) to films, despite the limitation of the small precursor amount in films, which pushes TA techniques to their limits. We will provide a closer look at the pyrolysis of FF-$YBa_2Cu_3O_{7-\partial}$ (YBCO) films [27,28], a high temperature superconductor (HTS)[29,30], by studying in-situ the effect of TEA on each of the three metalorganic salts used for the fabrication of YBCO with chemical methods: yttrium propionate ($YProp_3$) [22,24,31,32], copper propionate ($CuProp_2$) [20,33–35] and a mixed barium propionate-acetate salt

($Ba_7Prop_8Ac_6$, also labelled as Ba-Prop-Ac) [18]. Humid O_2 atmospheres will be studied in comparison to inert atmospheres, as the former are normally used during YBCO pyrolysis. Evolved gas analysis (EGA-FTIR and EGA-MS) coupled to TG-DSC will be used to reveal the gas species evolved during decomposition. XRD, FTIR and EA will be used to characterize ex-situ the solid residue at different stages of the thermal degradation. We will show that TEA changes the decomposition mechanism of the carboxylate salt, and that it can affect the final products in terms of amount of carbon. Finally, we will use TA to discuss decomposition in the context of the nature of TEA interaction with the metalorganic salt.

• Materials and methods

2.1 Sample preparation

Three separate solutions were prepared starting from metal acetate precursors. $Y(CH_3CO_2)_3$ (YAc_3, Sigma Aldrich, 0.25M), $Ba(CH_3CO_2)_2$ ($BaAc_2$, Sigma Aldrich, 0.5M) and $Cu(CH_3CO_2)_2$ ($CuAc_2$, Alfa Aesar, 0.75M) were separately dissolved in a 1/1 mixture of propionic acid (Merck, ≥99%) and MeOH (VWR, ≥99.8%). Replacement of acetate groups by propionate is expected to take place in these solutions [18,24–26,36,37], in particular a complete replacement for the Cu and Y salts and partial for the Ba salt. Note that the Y/Ba/Cu metal ratio from the three solutions is of 1/2/3 (sol. **A**, **B** and **C**, respectively). A 5% v/v of triethanolamine (TEA, Merck, >99%) was added to each solution so that the final molar proportions Y/Ba/Cu/TEA were close to 1/2/3/1.5. For comparison, solutions without propionic acid were prepared from the corresponding metal propionate salts ($MProp_x$) obtained by drying the previous solutions (**A** and **C**); these $MProp_x$ salts were dissolved in MeOH with 5% TEA, maintaining the same stoichiometric ratio: **A'** ($YProp_3$/TEA in MeOH) and **C'** ($CuProp_2$/TEA in MeOH). Films were prepared from these solutions by drop casting over 10x10 mm $LaAlO_3$ (LAO) substrates. They were dried at 80°C for a few minutes to remove most of the solvent while avoiding TEA evaporation. After this stage, for the Y/TEA and Ba/TEA case the film has a gel-like aspect, while the Cu/TEA sample is drier. Some of these films were then decomposed in humid O_2 during thermal analysis experiments, while others were peeled off and the material was placed in a 70-µl alumina pan to study its decomposition in inert atmosphere. The latter will be referred to as "powders" to differentiate their geometry from that of the films. The film thickness (H) was estimated with the following equation:), where *m* is the film mass after decomposition, *d* is the particle density of Y_2O_3, CuO or $BaCO_3$, and *A* is the substrate area.

2.2 Characterization methods

Thermogravimetric (TG) analyses were performed in a Mettler-Toledo thermobalance, model TGA/DSC1, at 5°C/min. Experiments performed in humid O_2 atmosphere were carried out with a 55-ml/min flow of reactive gas (humid O_2) and 15 ml/min of protective gas (air). The reactive gas was humidified by bubbling it in a

water flask at standard temperature and pressure (25°C, 1 atm). Under these conditions the water vapor partial pressure is 3.1% [38] . Experiments run in N_2 atmosphere were performed with flow rates of 70 ml/min of the dry inert gas.

TG-FTIR experiments were carried out connecting the gas outlet of the TG equipment to the gas inlet of an infrared (IR) spectrometer with a 30-cm steel tube. The IR analyzer was a Bruker Alpha II spectrometer equipped with a gas cell. Both gas cell and steel tube were kept at 200°C to prevent volatile condensation. Experiments were recorded with an acquisition time of 30 seconds/spectrum and a spectral resolution of 4 cm^{-1}. Identification of gaseous infrared spectra is based on refs. [16,39].

EGA-MS experiments were run placing the film on an alumina holder inside a quartz tube closed on one end. This quartz tube extremity is surrounded by a low-inertia furnace. A type K thermocouple was in tight contact with the film substrate and used to control the temperature program. The open end of the quartz tube was connected to the vacuum system and to a quadrupole mass spectrometer (MS-Q) analyzer by MKS instruments, model Microvision Plus. The vacuum was reached by pumping the system to P_{tot}~10^{-7} bar with the aid of a turbomolecular pump in series with a rotative pump. Identification of the volatiles from the MS analysis is based on [40].

Elemental analysis (EA) was performed with a Perkin Elmer EA2400 series elemental analyzer. Detection limits are in the range of 0.72% for C and 0.2% for H values. X-ray diffraction (XRD) measurements were carried out with a Cu-Kα X-ray beam of a D8 ADVANCE diffractometer from Bruker AXS, with a voltage of 40 kV and a 40-mA current. XRD patterns were identified based on refs. [26,41]. Infrared spectra of solid samples were collected with an ALPHA spectrometer from Bruker, in attenuated total reflection (ATR, model Platinum), and the species identified according to [24–26,39].

• Results

- *Thermal decomposition of Ba-Prop-Ac /TEA (sol. **B**)*

The Ba-Prop-Ac/TEA solution (sol **B**) exhibits the simplest behavior of the three under study, and for this reason is discussed first. The FTIR spectra in Fig. 1a of the dry films show characteristic TEA vibration bands, and the partial replacement of acetate groups by propionates [42] with formation of a mixed Ba-Prop-Ac complex [18,26]. The XRD of the dry film (Fig. 1b) is in agreement with that of the mixed carboxylate salt, $Ba_7Prop_8Ac_6$, found in [26], suggesting that no new TEA-Ba complex is formed.

The thermogravimetric curve shown in Fig. 2 displays three main mass-loss steps: the first, between 50 and 200°C, corresponds to water and propionic acid evaporation; the second, between 150 and 300°C, corresponds to the loss of TEA groups; and the third, between 300 and 500°C, is the decomposition of Ba-Prop-Ac.

The second TG step has a 27.7% mass loss, very close to the theoretical value

for TEA removal (29.28% starting from $Ba_7Prop_8Ac_6$). In the 150-210°C range a gradual mass loss takes place while the FTIR curve of the solid residue at 210°C (Fig. 1) reveals that during TEA evolution, an IR band at 1735 cm^{-1} emerges. This band can be assigned to an ester bond between propionic acid and TEA's OH groups. Indeed, this band also appears in a solution of only TEA and propionic acid (see Supp. Info, Fig. S1).

Since the decomposition study relative to the barium carboxylate salt [26] revealed that propionic acid from the solution can evolve up to 150-200°C, it is reasonable to believe that the propionate units involved in the esterification come from the solvent. In fact, if they came from the salt, the mass after the loss of TEA would be smaller than that of Ba-Prop-Ac, in contradiction to the experimental results (Fig. 2). An endothermic DSC signal centered at 220°C (Fig. 2) is also consistent with some TEA evaporation, in agreement with the temperature range observed for TEA evaporation in films in ref. [16]. However, it was not possible to identify the TEA by TG-FTIR analysis in the gas phase due to the small amount evaporating, which was further reduced by its condensation along the path, a phenomenon already noted in ref. [16]. Additionally, between 210 and 300°C, the high temperatures promote TEA decomposition and, in fact, the infrared analysis of the gaseous species shows TEA's decomposition products: ammonia and acetaldehyde (TG-FTIR in inset of Fig. 2).

Between 210 and 280°C, the XRD curves (Fig. 1b) show a shift in the peaks between 5 and 10 deg., indicating a change in the barium carboxylate structure which takes place during TEA removal. As expected, its carboxylic stretching bands have also shifted from 1512 cm^{-1} to 1549 cm^{-1} between 210 and 280°C before oxidative degradation begins (Fig. 1b). Both effects observed before 300°C by XRD and FTIR analysis were also noticed for the barium propionate-acetate salt alone, and attributed to dehydration, recrystallization and melting of the salt [26]. The main TEA absorptions and the ester peak disappear after this stage, leaving an FTIR spectrum at the beginning of the third stage (280°C) that is identical to that of the barium carboxylate salt at this temperature [26].

The third TG step in Fig. 2 corresponds to the decomposition of Ba-Prop-Ac to $BaCO_3$, with a characteristic DSC exothermic peak [26] and with a $m_{500°C}/m_{300°C}$ ratio of 71.2% for this step (theoretical of 72.7% starting from $Ba_7Prop_8Ac_6$). Acetaldehyde, CO_2, methane and CO are detected in humid O_2, in agreement with [26].

The expected final mass with respect to the initial dry film considering a simple addition of all components in solution (Ba-Prop-Ac + TEA) is of 51.41%, in agreement with the thermogravimetric curve which lies at 51%. EA results in Table 1 at 500°C shows a C% value slightly above the expected one for $BaCO_3$, which might indicate that the gray color of the final product (expected to be white) is due to residual carbon remaining, just as in the case of Ba-Prop-Ac alone. With respect to Ba-Prop-Ac alone (see Supp. Info, Fig. S4), the thermogravimetric behavior is very similar, as well as the final decomposition temperature. Also, the EGA-MS analysis of

a film of solution **B** decomposed in vacuum (See Supp. Info, Fig. S8) yields identical results to the EGA-MS of Ba-Prop-Ac without TEA [26], confirming that TEA evaporation in vacuum takes place before the salt decomposition.

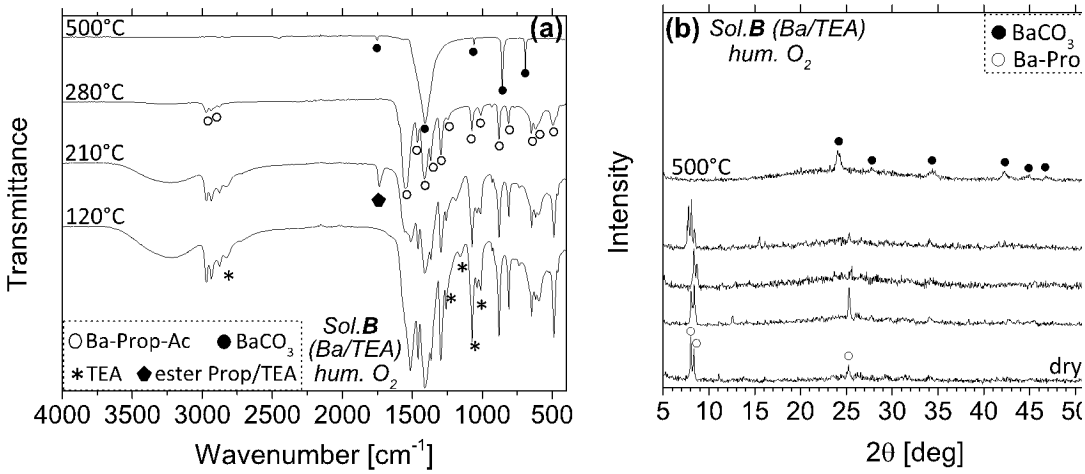

Fig. 1: (a) FTIR analysis and (b) XRD pattern of some quenched films during decomposition of sol. **B** (Ba/TEA) in humid O_2 at 5°C/min.

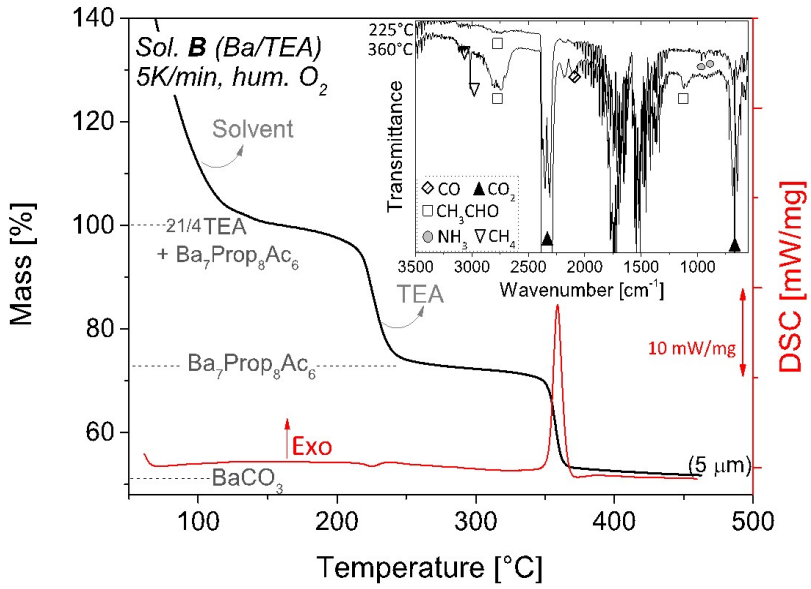

Fig.2: TG-DSC analysis of Ba-Prop-Ac/TEA film (~5 µm from sol. **B**) decomposition in humid O_2 at 5°C/min. Inset: Infrared spectra of gas species detected from TG-FTIR analysis. Horizontal dashed lines: theoretical final mass of the indicated species.

Compound	Found (expected), mass %	
	wt%C	wt%H

A (Y/TEA, 600°C)	1.3 (0)	- (0)
A (Y/TEA, 500°C)	2.6	0.4
B (Ba/TEA, 500°C)	6.7 (6.09)	- (0)
C (Cu/TEA, 500°C)	- (0)	- (0)

Table 1: Elemental analysis results for the decomposition products of metal carboxylate/TEA solutions in humid O_2. (-) values inferior to detection limits. Expected values correspond to yttria, barium carbonate and copper oxide.

- *Thermal decomposition of $CuProp_2$ /TEA (sol. **C**)*

Decomposition in oxidative atmosphere

The FTIR analysis of the dry film from solution **C** (Fig. 3a) shows the appearance of the TEA IR bands and of $CuProp_2$ vibrations [20,25,43], in agreement with the expected replacement of acetate groups by propionates of the solvent when this is in excess [42] (details in Fig. S2). However, the XRD pattern is significantly different from that of $CuProp_2$ [25] (see Fig. S2), suggesting a possible coordination of TEA with $CuProp_2$.

The TG analysis in humid O_2 reported in Fig. 4 shows that, after solvent removal and dehydration, which occur below 150°C, four overlapping steps centered at 155, 210, 245 and 328°C take place. They correspond to exothermic processes (DSC signal in Fig. 4, top). The gas species evolved consist of propionic acid, acetaldehyde, CO_2 and NH_3 (Fig. 4). Since only NH_3 can be easily assigned to TEA decomposition, while all other gas species are the expected volatiles for both TEA and for $CuProp_2$ decomposition, interpretation of the TG-FTIR results is not straightforward.

The four mass steps can be grouped into two main stages. During the first stage, between 100 and 230°C, $CuProp_2$ decomposes to Cu and Cu_2O, and some TEA is released. During the second stage, from 230 to 360°C, the remaining TEA decomposes.

Concerning the first stage, $CuProp_2$ decomposition and TEA removal are revealed by XRD and FTIR analysis (Fig. 3). The FTIR (Fig. 3a) of the solid residue quenched at 185°C shows that the main TEA vibrational band at ~1082 cm^{-1} is decreasing; simultaneously, the $CuProp_2$ reflections appear in the XRD of the solid

residue (Fig. 3b) [25,44] and as $CuProp_2$ decomposes in this stage they disappear around 230°C. The FTIR curve at 230°C still reveals the presence of TEA and some $CuProp_2$ (Fig. 3) but the latter is residual since it is not observed by XRD. Decomposition of $CuProp_2$ occurs according to the expected hydrolysis and degradative oxidation path [25] through the formation of propionic acid and CO_2 (TG-FTIR analysis in Fig. 4). Between 95 and 185°C, an IR band at 1735 cm^{-1} appears in the solid residue, Fig. 3a, which may be assigned to the TEA/propionate ester bond, although a similar absorption band was observed for the $CuProp_2$ decomposition in correspondence with its reduction to Cu(I). At 230°C, the only phases observed by XRD are Cu and Cu_2O. Reduction of Cu(II) to Cu(I) and Cu(0) is favored by the presence of TEA, and the peak relative to CO_2 evolution at ~210°C (Fig. 4) could be an indication of the redox reaction between Cu(II) and carbon left by TEA.

Concerning the second stage, TEA experiences an oxidative decomposition which produces CO_2, acetaldehyde and NH_3 as volatiles, detected between 210-270° C (Fig. 4). Since a $CuProp_2$ film without TEA is fully decomposed at 250°C in O_2 (see Fig. S4), the last evolution of CO_2 centered at 328°C is directly attributable to TEA oxidation. In fact, a TG-FTIR experiment run on TEA alone (Fig. S9) reveals that the degradation of TEA in oxygen continues above 300°C. Finally, the temperature range of this second TG stage is also in agreement with the decomposition temperatures found for other Cu-TEA complexes [9,17,45,46]. The residual $CuProp_2$ at 230°C, observed by FTIR in Fig. 1a, disappear during this stage, most probably between 230-250°C; in fact, part of the acetaldehyde and CO_2 detected by TG-FTIR between 230-250°C can also be attributed to this process.

The final product consists of CuO, as shown by XRD and FTIR in Fig. 3, and no carbon or hydrogen is detected by EA (Table 1). The experimental final mass lies at 32%, slightly above the expected value of 28.9 %. A solution of $CuProp_2$ with 5% TEA in only MeOH (sol. **C'**) yields the same TG-FTIR behavior and for comparison it is shown in Fig. 4.

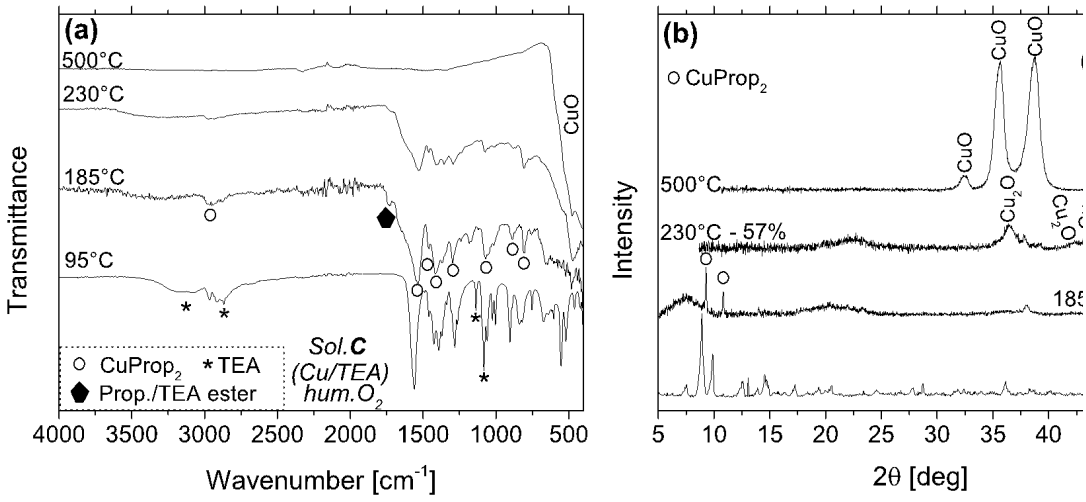

Fig.3: Chemical characterization of quenched samples during the thermal decomposition of $CuProp_2$/TEA (sol. **C**) at 5°C/min in humid O_2. (a) FTIR analysis and (b) XRD patterns.

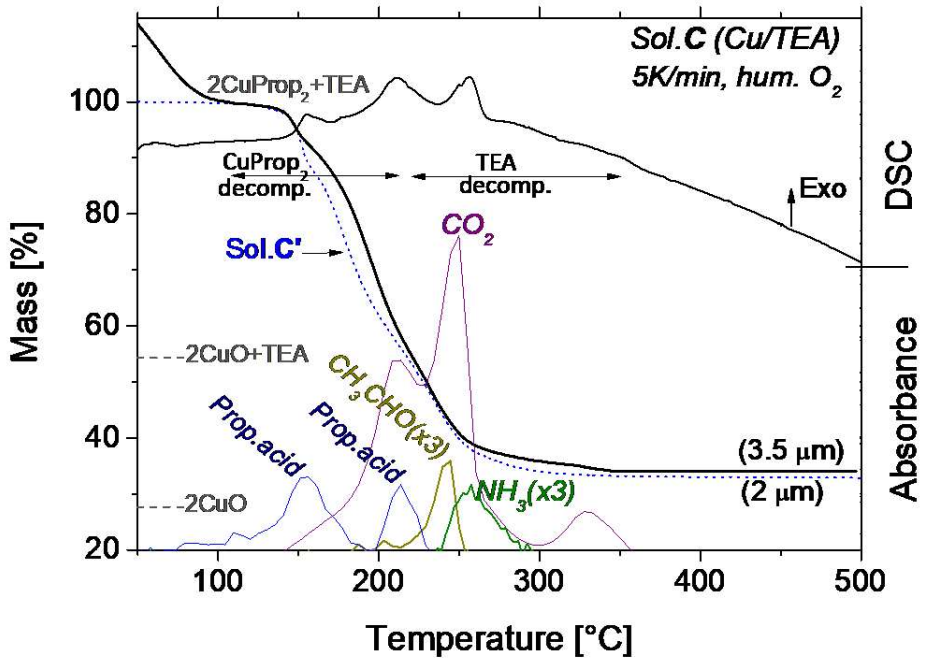

Fig.4: TG-DSC-FTIR analysis of $CuProp_2$/TEA film (sol. **C**) decomposed in humid O_2 at 5°C/min. Dotted line: TG curve relative to sol. **C'**. The absorbance peaks are plotted choosing the evolution in temperature of a characteristic wavenumber for each volatile. Horizontal dashed lines: theoretical final mass for the formation of the indicated products.

Decomposition in inert atmosphere

It is known that both $CuProp_2$ [25] and TEA independently exhibit a strong tendency to evaporate at low total pressure. However, when decomposition of solution **C** is carried out in vacuum $CuProp_2$, evaporation is considerably reduced. In fact, unlike the case of $CuProp_2$ alone in the form of film, with the addition of TEA, $CuProp_2$ does not condensate along the quartz tube, and the mass loss is very similar to the expected value. The final product at 500°C consists of a shiny metallic copper film, indicating that $CuProp_2$ evaporation is definitely reduced in vacuum when TEA is added.

In the EGA-MS analysis (Fig. 5), only a low-temperature stage is observed. The most intense peak still shows the evolution of propionic acid (m/z=45, 29, 28, 27) at 200°C coming from $CuProp_2$ decomposition. However, an excess of m/z=28 (CO, N_2 or C_2H_4) with respect to the case without TEA is observed. This may be an indication that TEA is present up to 200°C, and consequently that also its evaporation is reduced when $CuProp_2$ is added, due to the coordination between TEA and the Cu^{2+} of the carboxylic salt. To better understand the thermal decomposition of sol. **C** in inert atmosphere, the effect of evaporation should be minimized by studying decomposition *i)* in powder instead of film and *ii)* at the atmospheric pressure of an inert gas, such as N_2, instead of in vacuum.

The TG behavior during decomposition in N_2 of the powder obtained from solution **C** is reported in Fig. 5. Exothermic events are still observed in the first stage, before 230°C, in correspondence with propionic acid and CO_2 release coming from the beginning of $CuProp_2$ decomposition in N_2. The main difference from the humid-O_2 case lies in the formation of a TEA-propionate ester evolving at 260°C, in the second stage. This ester is ethyl propionate, detected among the volatiles by TG-FTIR (inset in Fig. 5) along with some TEA, while the CH_3CHO and NH_3 that would come from TEA decomposition alone are no longer detected.

This ester (ethyl propionate) comes from a decomposition process. Thus, it is different from the ester observed by FTIR (band at 1735 cm^{-1}) in the solid residue at low temperatures in sol. **B** (Fig. 1a) and in sol. **A**, (see later in section 3.3), which instead comes from the esterification between TEA and propionic acid as solvent (see also Fig. S1). This difference will be further discussed in section 3.3, for the case of sol. **A**. Indeed, ethyl propionate can be ascribed to the decomposition path described by the following reaction scheme:

$$N(C_2H_4OH)_3 + M(C_2H_5CO_2)_x \;\; xC_2H_5C(=O)–OC_2H_5 + MO_x + N_2 \qquad (i)$$

Where M is the metal cation (Cu or Y).

Note that, in vacuum, formation of ethyl propionate is probably disfavored by the low decomposition temperature (200°C - Fig. 5, bottom) and the tendency for both TEA and $CuProp_2$ to evaporate at low total pressures. Note also that, in N_2, $CuProp_2$ in powder form without TEA decomposes with a sharp mass loss followed by the reduction of copper to Cu(0) (see Fig. S4 and [25]). In contrast, the overlapped decomposition of TEA and the carboxylic salt, which results in the

occurrence of reaction scheme *(i)*, makes decomposition of sol. **C** smoother.

Finally, note that, according to reaction scheme *(i)*, the generation of ethyl propionate as a volatile is consistent with the formation of CuO instead of Cu. Indeed, in the same decomposition conditions (powders in N_2) only Cu and Cu_2O are observed during decomposition of $CuProp_2$ without TEA [25] at 360°C. Conversely, during decomposition of $CuProp_2$ with TEA, CuO is also detected at 360°C (sol. **C**, see Fig. S3 in supp. Info), indicating that less reduction occurs at intermediate temperatures. It is reasonable to believe that when TEA and $CuProp_2$ decompose simultaneously, forming the ester (stage II of Fig. 5) instead of propionic acid, the occurrence of reaction scheme *(i)* prevents Cu(II) reduction in N_2.

Once formed, this copper oxide is eventually reduced to Cu(0) in inert atmosphere, further aided by the residual carbon, which evolves as CO_2. CO_2 is indeed detected between 480-500°C (see inset in Fig. 5). The final mass lies at 29.6%, higher than the expected value for Cu, indicating presence of residual carbon, just as found for the case of the thermal decomposition of powders of $CuProp_2$ in N_2 [25].

Thus, the formation of ethyl propionate requires higher temperatures than the low-temperature range (100-200°C, Fig. S4 in Supp. Info) where $CuProp_2$ is expected to decompose in O_2, and for this reason, its contribution to decomposition in humid O_2 is minor (and propionic acid remains the main volatile). Due to the fact that an increase in $CuProp_2$ film thickness causes a shift of decomposition to higher temperatures [25], some ethyl propionate is in fact detected even in humid O_2 above 200°C, for CuO films thicker than 4 µm (see Fig. S7). This suggests that even for films thinner than 4 µm, in humid O_2, the ethyl propionate path could occur above 200°C, but it is inhibited by the humid atmosphere, probably resulting in the formation of the second propionic acid peak of Fig. 4, above 200°C. Finally, even increasing the TEA/Cu ratio in solution to 1/1 in order to push the equilibrium towards the ester instead of towards propionic acid is unsuccessful: the main volatile in humid O_2 is still propionic acid (not shown).

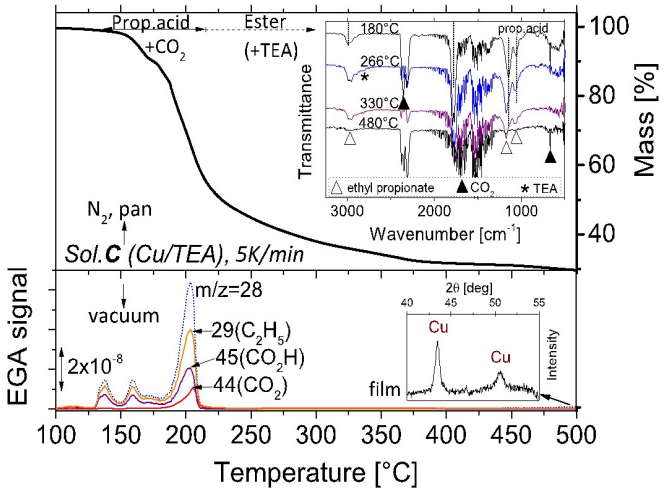

Fig.5: (top graph) TG-FTIR analysis of 25-mg powders from sol. **C** decomposed in N_2 at atmospheric pressure (details in Supp. Info, Fig. S6); (bottom graph) EGA-MS analysis of a film from sol. **C** showing the main fragments coming from decomposition in vacuum of $CuProp_2$/TEA at 5°C/min.

- *Thermal decomposition of $YProp_3$ /TEA (**A**)*

Decomposition in oxidative atmosphere

As deduced from the TG curve of Fig. 6, solution **A** is hard to dry at low temperature, since evaporation and decomposition overlap. After drying at 80°C, the film is still a colorless, viscous liquid; the FTIR spectrum of Fig. 7a shows the TEA IR bands and those of $YProp_3$ ([24] and Fig. S2). To remove the contribution of the solvent and for clarity, the time-resolved evolution of the volatiles reported in the TG-FTIR analysis of Fig. 6 (dotted lines) is relative to solution **A'**. In fact, **A'** is prepared by dissolving $YProp_3$ in MeOH, while **A** is prepared by dissolving YAc_3 in a mixture of propionic acid and MeOH. For both **A** and **A'**, the expected final mass for the mixture of $YProp_3$ and TEA to yield Y_2O_3 is 21.2%, which is in agreement with the experimental value of 24.5% of Fig. 6, considering that the FTIR analysis (Fig. 7a) of the solid residue at 600°C reveals the presence of residual Y-oxycarbonate, $Y_2O_2CO_3$.

Three main stages can be identified when decomposition is carried out in humid O_2.

The first stage, between 50 and 150°C (Fig. 6), involves the dehydration and evaporation of the solvent (propionic acid). In fact, in the solid residue (Fig. 7a) the main propionic acid and H_2O IR absorptions decrease as temperature rises from 90°

C to 150°C. In particular, the disappearance of the broad band between 2500-400 cm^{-1} is a sign of solvent removal, but the general intensity decrease in the 1300-1700 cm^{-1} region (where the $YProp_3$ bands are found) is due to the solvent as well. This step also corresponds to the appearance of an ester band at 1736 cm^{-1} in the FTIR of the solid residue, the same band also noticed for sol. **B**. This band probably arises because the temperature increase promotes esterification between TEA and propionic acid. In **B** this was explained by the fact that no coordination took place between TEA and Ba ions, thus all TEA (Ba/TEA=2/1.5) is free to react with the solvent (prop. acid). In sol. **A**, there is always some free TEA since TEA is in excess with respect to Y^{3+} (Y/TEA=1/1.5). Conversely, esterification of the solvent in **C** is minor, because Cu is in excess with respect to TEA, and TEA is coordinated to $CuProp_2$.

The second stage, between 150-300°C, corresponds to a 37% mass loss. The main volatiles detected are propionic acid and ethyl propionate, but TEA's vibrational bands [16] are observed as well. The propionic acid comes from $YProp_3$ decomposition in humid O_2; ethyl propionate, already observed also for solution **C**, originates from the simultaneous decomposition of both TEA and $YProp_3$ according to reaction scheme (*i*). In fact, the IR bands in the solid residue (Fig. 7a) relative to yttrium propionate decrease monotonously up to 240°C. The FTIR analysis of the solid residue, in Fig. 7a, also reveals that the contribution of TEA disappears somewhere between 240 and 340°C. The fact that TEA's vibrational bands are also observed among the volatiles is in agreement with the fact that evaporation takes place in films before 200°C and that there is an excess of TEA with respect to Y (1.5/1, respectively).

The last stage of Fig. 4.9, between 300-600°C, mostly includes $YProp_3$ decomposing to Y_2O_3, since most TEA has been previously consumed.

First, between 300 and 400°C, the remaining $YProp_3$ decomposes to $Y_2O_2CO_3$, observed by FTIR in Fig. 7a and in agreement with previous studies [21,24,31,32]. This process occurs upon release of CO_2, acetaldehyde and 3-pentanone (TG-FTIR in Fig. 6, top). Note that the CO_2 peaks between 300-330°C could also be ascribed to the end of TEA decomposition, since at higher temperatures its oxidative degradation takes place [16], releasing CO_2 (Fig. S9). However, the X-ray analysis reported in Fig. 7b shows the presence of amorphous species in this last stage (300-600°C), between $YProp_3$ decomposition and when Y_2O_3 crystallization takes place. Finally, between 400 and 500°C, $Y_2O_2CO_3$ decomposes to Y_2O_3 (identified by XRD, Fig. 7b) with CO_2 release. The EA results in Table 1 confirm the presence of carbon in the final product, due to residual $Y_2O_2CO_3$, similar to what occurs in the case of $YProp_3$ without TEA [24].

Note that, the ester band in the solid residue (~1736 cm^{-1}, Fig. 7a) disappears before 230°C, while ethyl propionate is detected among the volatiles between 200-350°C. As previously mentioned, these two esters are attributed to different processes. Ethyl propionate is ascribed to reaction scheme *(i)*. In fact, the boiling point of ethyl propionate is just below 100°C; thus, as soon as it is formed, it is expected to evaporate. Therefore, ethyl propionate cannot correspond to the ester

IR band of the solid residue at 1736 cm^{-1}. This band may arise majorly from the esterification of propionic acid (solvent) in the low-temperature region before its evaporation is completed.

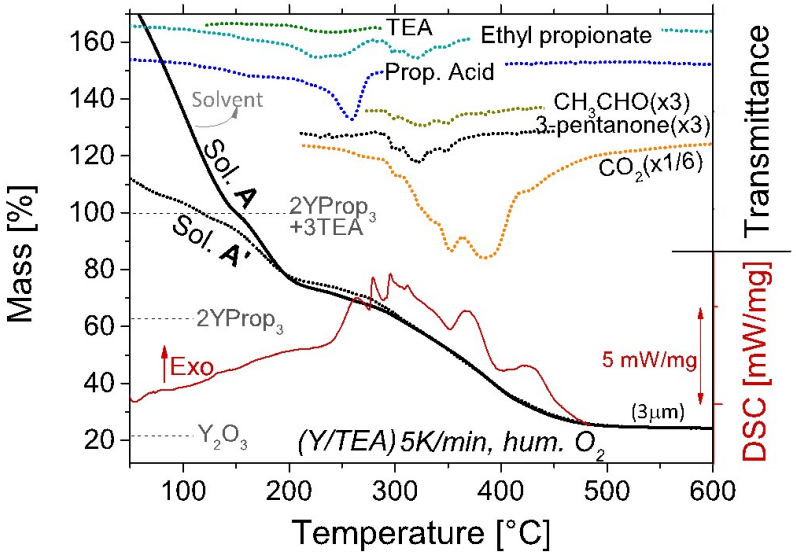

Fig. 6: TG-DSC analysis of $YProp_3$/TEA film from sol. **A** (solid lines) during decomposition in humid O_2 at 5°C/min, with the relative time-evolution of the main volatiles detected by TG-FTIR analysis from sol. **A'** (dotted line; the relative FTIR spectra at selected temperatures are reported in Fig. S5). Horizontal dashed lines: theoretical final mass for the formation of the indicated products.

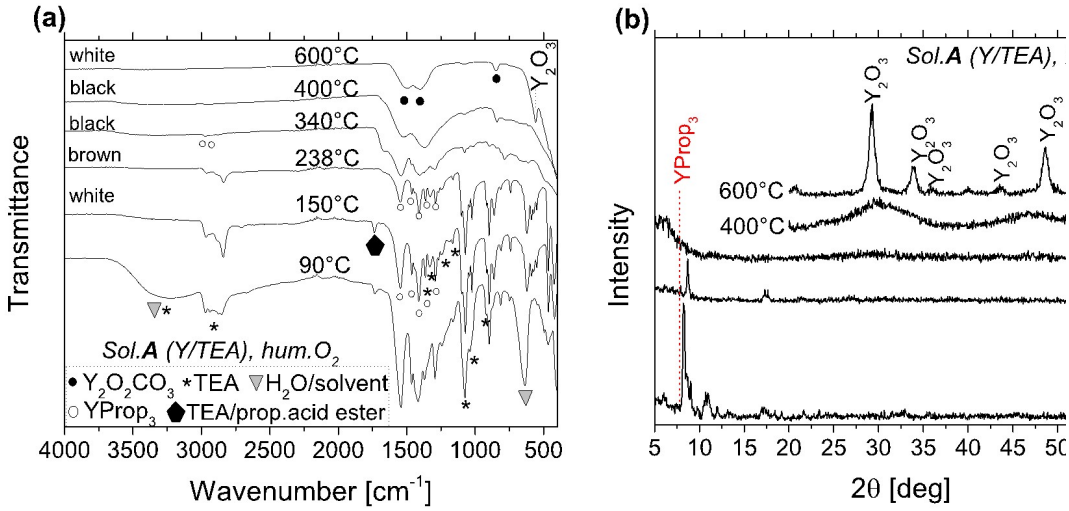

Fig. 7: (a) FTIR analysis and (b) XRD patterns of quenched samples during the thermal decomposition at 5°C/min and in humid O_2 of $YProp_3$/TEA (sol. **A**) shown in Fig. 6.

Decomposition in inert atmosphere

In inert atmosphere of N_2, decomposition of the powder sample from sol. **A** (Fig. 8) follows the same general behavior as films in humid O_2: TEA still evolves in the low-temperature stage at 250°C while CO_2 is detected at higher temperatures, namely 310, 340, 430°C, along with ethyl propionate.

However, the EGA-FTIR analysis of Fig. 8 (top, inset) shows that the ethyl propionate contribution increases in N_2. In fact, this ester becomes the main volatile, while the contribution of TEA and 3-pentanone decreases with respect to the film decomposition in humid O_2 (the only propionic acid detected seems to come from solvent evaporation below 200°C) and no ammonia coming from TEA decomposition can be detected. This is probably related to three facts. First, the lack of oxygen delays precursor decomposition, resulting in a major overlap of TEA and $YProp_3$ decomposition, which, in turns, favors esterification. Secondly, the powder form prevents TEA volatilization, which results again in a major overlap of TEA and $YProp_3$ decomposition. In fact, the two TG curves of sol. **A** (hum. O_2 and N_2) that are compared in Fig. S4, are quite similar, but the first mass loss (due to loss of TEA) is shifted to lower temperatures in films in humid O_2, since in films volatilization is enhanced with respect to decomposition. Third, reaction scheme (i) occurs through a radical reaction, which is favored by inert furnace atmospheres.

Therefore, reaction scheme *(i)* summarizes the driving reaction for decomposition of TEA/$MProp_x$ species in N_2.

The EGA-MS analysis in the bottom panel of Fig. 8, performed on a film of sol. **A** decomposed in vacuum, supports the TG-FTIR results. It shows the presence of at least 2 stages of decomposition between 250-400°C, while for the $YProp_3$ alone only one stage is present (at 360°C) [24]. The two peaks, centered at 280 and 360°C, include fragments that can be related to both ethyl propionate (m/z=29, 57) and 3-pentanone (m/z=57,29); however, they both show the evolution of CO_2 (m/z=44), a signature of the occurrence of the 3-pentanone decomposition path typical of $YProp_3$ in vacuum [21,24]. Then, at 400°C, the m/z=28 fragment is detected, which could be assigned to C_2H_4, N_2 or CO. This excess of m/z=28 is not detected during the decomposition of $YProp_3$ without TEA in vacuum. Thus, it is an indication that less evaporation of TEA occurs at these low total pressures as a consequence of its coordination with the metal carboxylate salt. The FTIR of the final product shows residual -C=O bands (probably from $Y_2O_2CO_3$), and is very similar to that of the isolated $YProp_3$ decomposed in vacuum [24].

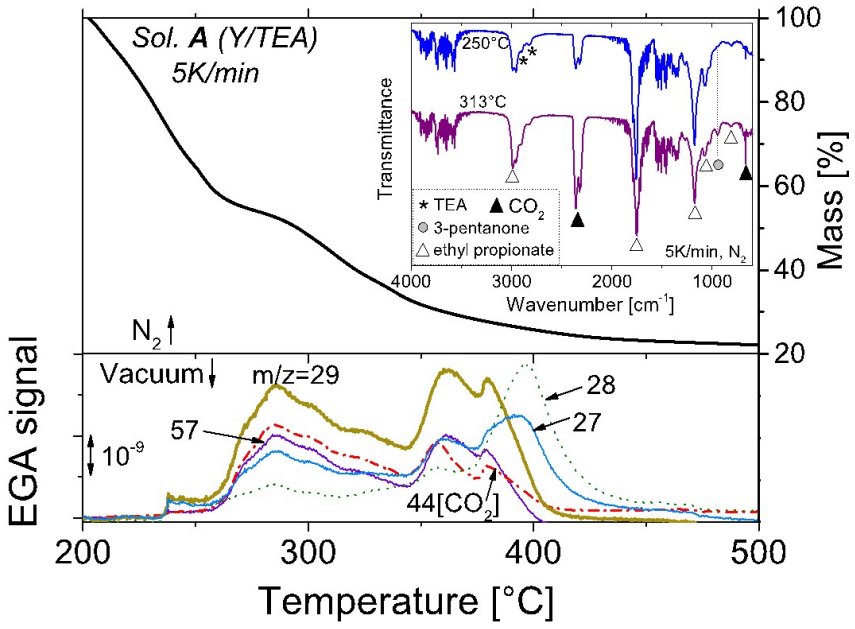

Fig. 8: TG-FTIR (top graph, with FTIR spectra in inset) and EGA-MS results (bottom) relative to the thermal decomposition of $YProp_3$/TEA (sol. **A**) at 5°C/min in N_2 (as powders, 15 mg) and vacuum (as film), respectively. Detailed IR spectra and enlargement of inset can be found in Fig. S6.

• Discussion

Thermal analyses provide useful information to understand the effect of adding TEA to the three different metalorganic solutions studied here.

In the case of Ba-Prop-Ac, the well-defined TG mass losses, the detection of TEA or its decomposition products among the volatiles, the endothermic signal of the TEA evaporation step and the same TG, EGA-MS behavior, and final decomposition temperature with and without TEA, all suggest that there is no coordination with TEA, as predicted in [12].

Conversely, TEA changes Cu and Y decomposition pathways, partly because of TEA coordination with Y and Cu, and partly because of the overlap of the decomposition of the metalorganic salt and the decomposition of TEA (the barium salt decomposes at higher temperatures), which results in less separable mass losses.

The decomposition mechanism derives from the tendency to break either the Cu—OC=O bond to form the corresponding acid, or the YO—C=O bond for the esterification reaction. In fact, for the copper case, the low-temperature mechanism with propionic acid formation is still faster and preferred in humid O_2, thus $CuProp_2$ decomposition is almost over when TEA decomposition begins. On the other hand, in N_2, $CuProp_2$ can survive to higher temperatures (260°C) for the ester to be produced. For the $YProp_3$ case, since its decomposition temperature is higher than that of $CuProp_2$ in humid O_2, esterification is more significant. This ester is not

observed in TEA decomposition alone [16], nor is it formed in the TEA-free solutions of the three metalorganic salts [24,25]. The oxidative degradation of the barium salt relies on the preferred cleavage of the MOC(=O)—C bond, as it tends to form BaC_2O_4 and $BaCO_3$ which only later (T>>600°C) decomposes to BaO [18,47]. This, and the fact that its decomposition temperature and TEA's are so far apart, makes it difficult to form the ethyl propionate ester.

It follows that the atmosphere has a different effect on decomposition when TEA is added to the carboxylate salt, since it changes the decomposition temperature range of the carboxylate salt, while it has no effect on the evaporation of TEA; i.e., it controls the overlap of the two processes (decomposition of TEA and of the salt) which eventually affects the degree of esterification and the decomposition pathway. Similarly, the sample geometry, film or powder, can promote or impede, respectively, evaporation of TEA, and thus control the overlap of the two processes.

However, the change in decomposition temperature due to a change of atmosphere is more significant for the pyrolysis of the single-salt solutions without TEA than for those with TEA. This is probably a consequence of the fact that the esterification path can also partly take place in humid O_2, although in dry N_2 it is the predominant decomposition path.

In the framework of CSD methods used to prepare oxide films, some effects need to be acknowledged when TEA is added. A shift of 100°C and 50°C for the Cu and Y case, respectively, can be observed in the final decomposition temperature with respect to the metalorganic salt without TEA; a slightly higher amount of residual carbon may remain at 600°C for the Y case, in humid O_2. The use of higher gas flows and targeted temperature profiles with slower heating ramps or isotherms is recommended to help complete decomposition at lower processing temperatures, of typically 400-500°C. Additionally, the presence of TEA causes an unexpected redox-reaction pattern not observed for the $CuProp_2$ alone [25]. In fact, reduction of Cu(II) occurs during decomposition in humid O_2 for sol. **C** ($CuProp_2$/TEA), due to the residual carbon from TEA; but this copper is eventually oxidized to CuO, which is the final product at 500°C in humid O_2. Conversely, in N_2, more Cu(II) reduction is expected during decomposition, but instead reaction scheme *(i)* generates CuO during pyrolysis; eventually this CuO undergoes reduction to Cu, which is the final product at 500°C.

Although only a fixed TEA amount was studied in this work, the M/TEA molar ratio may also play a role, influencing the amount of decomposition overlapping. In a combined solution of all the three salts analyzed, we would expect the TEA to influence the copper and yttrium carboxylate decomposition most of all. Perhaps the key aspect emerging from the thermogravimetric analysis is that, when TEA and the metal carboxylate display similar decomposition temperatures, the additive can provide smoother mass losses which translate into a gradual gas release. This is also reflected in the smaller effect of a change of atmosphere on the TG curves, unlike the case of the isolated salts. This smooth behavior justifies TEA application as a

solution stabilizer in thin film fabrication, based on the need to contrast the abrupt film shrinkage due to rapid decomposition. Likewise, the effect of switching from films to powders is less pronounced than for the isolated salts, although it is still evident from the fact that films in O_2 decompose earlier than powders, due to gas (i.e. O_2) depletion in the inter-particles voids of the bulk in the latter [48] (Fig. S10).

In the context of chemical solution deposition methods, where long-chain additives are used as stabilizers, the final decomposition temperatures and intermediate phases can play an important role in the final properties of the film, even when the final phases might not differ from the additive-free case.

• Conclusions

In conclusion, we have shown that thermal analysis can be used to study complex solution behavior even in the form of films. In a FF-YBCO precursor solution with 5%TEA, TEA is expected to affect decomposition. Decomposition results in the formation of ethyl propionate in inert atmosphere, for both yttrium propionate and copper propionate. This reaction path prevents CuO reduction to Cu(0) in N_2. In humid atmosphere, the different behavior of the two metal carboxylates is revealed through the formation of the ester for yttrium propionate and the formation of the corresponding acid for copper propionate, as a consequence of the preferred cleavage of the M—OC=O bond.

Although TEA is responsible for smoother mass losses when its decomposition temperature overlaps with that of the metal carboxylate, or when it is coordinated in a metalorganic complex, other effects need to be taken into account. For example, the presence of TEA shifts the final decomposition temperature to higher values for the copper and yttrium case in O_2, but not for the barium case. Residual carbon at 500-600°C might be more important when compared to metal carboxylate solutions without TEA. Additionally, if less “carbon” is added to the solution in the form of long chain additives, less Cu(II) reduction (in the form of Cu and Cu_2O) will take place in humid O_2 during decomposition.

Clearly this study deals with relatively thick films (>1 µm), but it can provide general guidelines for the study of YBCO obtained from CSD methods although they are based on thinner films (≤1µm).

Acknowledgments

This work was funded by Ministerio de Ciencia, Innovación y Universidades (grant numbers RTI2018-095853-B-C21 and RTI2018-095853-B-C22), by the Center of Excellence Severo Ochoa (SEV-2015-0496), the Generalitat of Catalunya (2017-SGR-1519). It was also supported by the European Union through the projects Eurotapes (EU-FP7 NMP-LA-2012-280432) and Ultrasupertape (ERC ADG-2014-669504). S.R. wishes to thank the University of Girona for the IF-UdG PhD grant.

References

[1] X. Obradors, T. Puig, S. Ricart, M. Coll, J. Gazquez, A. Palau, X. Granados, Growth, nanostructure and vortex pinning in superconducting YBa2Cu3O7 thin films based on trifluoroacetate solutions, Supercond. Sci. Technol. 25 (2012) 123001. doi:10.1088/0953-2048/25/12/123001.

[2] A. Rahman, Z. Rahaman, N. Samsuddoha, A review on cuprate based superconducting materials including characteristics and applications, Am. J. Phys. Appl. 3 (2015) 39–56. doi:10.11648/j.ajpa.20150302.15.

[3] T. Puig, J.C. Gonzáles, A. Pomar, N. Mestres, O. Castaño, M. Coll, J. Gásquez, F. Sandiumenge, S. Piñol, X. Obradors, The influence of growth conditions on the microstructure and critical currents of TFA-MOD YBa2Cu3O7 films, Supercond. Sci. Technol. 18 (2005) 1141–1150. doi:10.1088/0953-2048/18/8/020.

[4] A. Pomar, J. Gutiérrez, A. Palau, T. Puig, X. Obradors, Porosity induced magnetic granularity in epitaxial YBa2Cu3O7 thin films, Phys. Rev. B. 73 (2006). doi:10.1103/PhysRevB.73.214522.

[5] E. Bartolomé, F. Gömory, X. Granados, T. Puig, X. Obradors, Universal correlation between critical current density and normal-state resistivity in porous YBa2Cu3O7−x thin films, Supercond. Sci. Technol. 20 (2007) 895–899. doi:10.1088/0953-2048/20/10/001.

[6] W. Wu, F. Feng, K. Shi, W. Zhai, T. Qu, R. Huang, X. Tang, X. Wang, J.-C. Grivel, Z. Han, A rapid process of YBa2Cu3O7−δ thin film fabrication using trifluoroacetate metal organic deposition with polyethylene glycol additive, Supercond. Sci. Technol. 26 (2013) 055013. doi:10.1088/0953-2048/26/5/055013.

[7] C. Ecjhao, K. Majid, R. Mushtaq, Synthesis, characterization and coordinating behaviour of aminoalcohol complexes with transition metals, E-Journal Chem. 5 (2008) S969–S979. doi:10.1155/2008/680324.

[8] A.A. Naiini, V. Young, J.G. Verkade, G. Hall, New complexes of triethanolamine (TEA): novel structural features of [Y(TEA)2](ClO4)3•3C5H5N and [Cd(TEA)2](NO3)2, Polyhedron. 14 (1995) 393–400. doi:10.1016/0277-5387(95)93020-2.

[9] K.H. Whitmire, J.C. Hutchison, A. Gardberg, C. Edwards, Triethanolamine complexes of copper, Inorganica Chim. Acta. 294 (1999) 153–162. doi:10.1016/s0020-1693(99)00274-1.

[10] B. Kozlevčar, P. Šegedin, Structural analysis of a series of copper(II) coordination compounds and correlation with their magnetic properties, in: Croat. Chem. Acta, 2008: pp. 369–379.

[11] R.M. Escovar, J.H. Thurston, T. Ould-ely, A. Kumar, K.H. Whitmire, Synthesis and characterization of new mono-, di-, and trinuclear copper(II) triethanolamine-carboxylate complexes, Z. Anorg. Allg. Chem. 631 (2005) 2867–2876. doi:10.1002/zaac.200500204.

[12] K.D.B.Æ.P. Lommens, Æ.J.F.Æ.D. Vandeput, I. Van Driessche, Sol-gel chemistry

of an aqueous precursor solution for YBCO thin films, J. Sol-Gel Sci. Technol. 52 (2009) 124–133. doi:10.1007/s10971-009-1987-1.
[13] B. Schoofs, D. Van de Vyver, P. Vermeir, J. Schaubroeck, S. Hoste, G. Herman, I. Van Driessche, Characterisation of the sol-gel process in the superconducting NdBa2Cu3O7-y system, J. Mater. Chem. 17 (2007) 1714–1724. doi:10.1039/b614149h.
[14] S.G. De de Ávila, M.A. Logli, J.R. Matos, Kinetic study of the thermal decomposition of monoethanolamine (MEA), diethanolamine (DEA), triethanolamine (TEA) and methyldiethanolamine (MDEA), Int. J. Greenh. Gas Control. 42 (2015) 666–671. doi:10.1016/j.ijggc.2015.10.001.
[15] S.B. Fredriksen, K. Jens, Oxidative degradation of aqueous amine solutions of MEA, AMP, MDEA, Pz: a review, Energy Procedia. 37 (2013) 1770–1777. doi:10.1016/j.egypro.2013.06.053.
[16] I. Zghal, J. Farjas, J. Camps, M. Dammak, P. Roura, Thermogravimetric measurement of the equilibrium vapour pressure : Application to water and triethanolamine, Thermochim. Acta. 665 (2018) 92–101. doi:10.1016/j.tca.2018.05.007.
[17] V.T. Yilmaz, Y. Topcu, A. Karadag, Thermal decomposition of triethanolamine and monoethanolethylenediamine complexes of some transition metal saccharinates, Thermochim. Acta. 383 (2002) 129–135. doi:10.1016/s0040-6031(01)00685-2.
[18] R.B. Mos, M. Nasui, T. Petrisor Jr, M.S. Gabor, R. Varga, L. Ciontea, T. Petrisor, Synthesis, crystal structure and thermal decomposition study of a new barium acetato-propionate complex, J. Anal. Appl. Pyrolysis. 92 (2011) 445–449. doi:10.1016/j.jaap.2011.08.007.
[19] Z. Lin, D. Han, S. Li, Study on thermal decomposition of copper(II) acetate monohydrate in air, J. Therm. Anal. Calorim. 107 (2012) 471–475. doi:10.1007/s10973-011-1454-4.
[20] M. Nasui, R.B. Mos, T. Petrisor Jr, M.S. Gabor, R.A. Varga, L. Ciontea, T. Petrisor, Synthesis, crystal structure and thermal decomposition of a new copper propionate [Cu(CH3CH2COO)2]·2H2O, J. Anal. Appl. Pyrolysis. 92 (2011) 439–444. doi:10.1016/j.jaap.2011.08.005.
[21] J. Grivel, Thermal decomposition of yttrium(III) propionate and butyrate, J. Anal. Appl. Pyrolysis. 101 (2013) 185–192. doi:10.1016/j.jaap.2013.01.011.
[22] J. Grivel, Thermal decomposition of lutetium propionate, J. Anal. Appl. Pyrolysis. 89 (2010) 250–254. doi:10.1016/j.jaap.2010.08.011.
[23] J. Grivel, Thermal decomposition of Ln(C2H5CO2)3•H2O (Ln=Ho,Er,Tm and Yb), J. Therm. Anal. Calorim. 109 (2012) 81–88. doi:10.1007/s10973-011-1745-9.
[24] S. Rasi, S. Ricart, X. Obradors, T. Puig, P. Roura, J. Farjas, Thermal decomposition of yttrium propionate: film and powder, J. Anal. Appl. Pyrolysis. 133 (2018) 225–233. doi:10.1016/j.jaap.2018.03.021.
[25] S. Rasi, F. Silveri, S. Ricart, X. Obradors, T. Puig, P. Roura-Grabulosa, J. Farjas, Thermal decomposition of CuProp2: In-situ analysis of film and powder pyrolysis, J. Anal. Appl. Pyrolysis. 140 (2019) 312–320. doi:10.1016/j.jaap.2019.04.008.

[26] S. Rasi, S. Ricart, X. Obradors, T. Puig, P. Roura-Grabulosa, J. Farjas, Radical and oxydative pathways in the pyrolysis of a barium propionate-acetate salt, J. Anal. Appl. Pyrolysis. 141 (2019) 104640. doi:10.1016/j.jaap.2019.104640.
[27] D.M. de Leeuw, C.A.H.A. Mutsaers, R.A. Steeman, E. Frikkee, H.W. Zandbergen, Crystal structure and electrical conductivity of YBa4Cu3O8.5+∂, Phys. C. 158 (1989) 391–396.
[28] P. Vermeir, I. Cardinael, J. Schaubroeck, K. Verbeken, B. Michael, P. Lommens, W. Knaepen, D. Jan, K. De Buysser, I. Van Driessche, Elucidation of the mechanism in fluorine-free prepared YBa2Cu3O7-δ coatings, Inorg. Chem. 49 (2010) 4471–4477. doi:10.1021/ic9021799.
[29] H. Maeda, Y. Yanagisawa, Recent developments in high-temperature superconducting magnet technology (Review), IEEE Trans. Appl. Supercond. 24 (2014) 1–12. doi:10.1109/TASC.2013.2287707.
[30] X. Obradors, T. Puig, Coated conductors for power applications: materials challenges, Supercond. Sci. Technol. 27 (2014) 44003–44019. doi:10.1088/0953-2048/27/4/044003.
[31] M. Nasui, T. Petrisor Jr, R.B. Mos, A. Mesaros, R.A. Varga, B.S. Vasile, T. Ristoiu, L. Ciontea, T. Petrisor, Synthesis, crystal structure and thermal decomposition kinetics of yttrium propionate, J. Anal. Appl. Pyrolysis. 106 (2014) 92–98. doi:10.1016/j.jaap.2014.01.004.
[32] M. Nasui, C. Bogatan (Pop), L. Ciontea, T. Petrisor, Synthesis, crystal structure modeling and thermal decomposition of yttrium propionate [Y2(CH3CH2COO)6·H2O]·3.5H2O, J. Anal. Appl. Pyrolysis. 97 (2012) 88–93. doi:10.1016/j.jaap.2012.05.003.
[33] M.S. Akanni, O.B. Ajayi, J.N. Lambi, Pyrolytic decomposition of some even chain length copper(II) carboxylates, J. Therm. Anal. 31 (1986) 131–143. doi:10.1007/bf01913894.
[34] M.D. Judd, B.A. Plunkett, M.I. Pope, The thermal decomposition of calcium, sodium, silver and copper(II) acetates, J. Therm. Anal. 6 (1974) 555–563. doi:10.1007/BF01911560.
[35] W. Yaoyu, S. Qianl, S. Qizhenl, G. Yici, Z. Zhongyuan, Synthesis , thermal decomposition and crystal structure of Copper (II) α, β-unsaturated carboxylate with urea, Chinese Sci. Bull. 44 (1999) 602–605. doi:10.1007/bf03182717.
[36] M. Nasui, T. Petrisor, R.B. Mos, M.S. Gabor, A. Mesaros, F. Goga, L. Ciontea, T. Petrisor, Fluorine-free propionate route for the chemical solution deposition of YBa2Cu3O7−x superconducting films, Ceram. Int. 41 (2015) 4416–4421. doi:10.1016/j.ceramint.2014.11.132.
[37] Y. Zhao, P. Torres, X. Tang, P. Norby, J. Grivel, Growth of highly epitaxial YBa2Cu3O7−δ films from a simple propionate-based solution, Inorg. Chem. 54 (2015) 10232–10238. doi:10.1021/acs.inorgchem.5b01486.
[38] O.C. Bridgeman, E.W. Aldrich, Vapor Pressure Tables for Water, J. Heat Transfer. 86 (1964) 279. doi:10.1115/1.3687121.
[39] W.E. Wallace, Infrared Spectra, in: P.J. Linstrom, W.G. Mallard (Eds.), NIST Chem. WebBook, NIST Stand. Ref. Database Number 69, Institute of Standards and Technology, Gaithersburg MD, 20899, n.d.

doi:https://doi.org/10.18434/T4D303.
[40] W.E. Wallace, Mass spectra, in: P.J. Linstrom, W.G. Mallard (Eds.), NIST Chem. WebBook, NIST Stand. Ref. Database Number 69, National Institute of Standards and Technology, Gaithersburg MD, 20899, n.d. doi:https://doi.org/10.18434/T4D303.
[41] R.T. Downs, M. Hall-Wallace, The American Mineralogist Crystal Structure Database, Am. Mineral. 88 (2003) 247,250.
[42] X. Palmer, C. Pop, H. Eloussi, B. Villarejo, P. Roura, J. Farjas, A. Calleja, A. Palau, T. Puig, S. Ricart, Solution design for low-fluorine trifluoroacetate route to YBa2Cu3O7 films, Supercond. Sci. Technol. 29 (2016) 24002. doi:10.1088/0953-2048/29/2/024002.
[43] J.A.R. Cheda, M. V García, M.I. Redondo, S. Gargani, P. Ferloni, Short chain copper(II) n-alkanoate liquid crystals, Liq. Cryst. 31 (2004) 1–14. doi:10.1080/02678290310001628500.
[44] Y.H. Chung, H.H. Wei, Y.H. Liu, G.H. Lee, Y. Wang, Reinvestigation of the crystal structure and cryomagnetic behaviour of copper(II) propionates, Polyhedron. 17 (1998) 449–455. doi:10.1016/s0277-5387(97)00367-7.
[45] H.Ö. H. Içbudak, V.T. Yilmaz, Thermal decompositions of some divalent transition metal complexes of triethanolamine, J. Therm. Anal. 44 (1995) 605–615. doi:10.1007/BF02636280.
[46] A. Karadag, V.T. Yilmaz, C. Thoene, Di- and triethanolamine complexes of Co(II), Ni(II) and Zn(II) with thiocyanate: synthesis, spectral and thermal studies. Crystal structure of dimeric Cu(II) complex with deprotonated diethanolamine, [Cu2(μ-dea)2(NCS)2], Polyhedron. 20 (2001) 635–641. doi:10.1016/S0277-5387(01)00720-3.
[47] P. Torres, P. Norby, J. Grivel, Thermal decomposition of barium valerate in argon, J. Anal. Appl. Pyrolysis 116. 116 (2015) 120–128. doi:10.1016/j.jaap.2015.09.018.
[48] P. Roura, J. Farjas, H. Eloussi, L. Carreras, S. Ricart, T. Puig, X. Obradors, Thermal analysis of metal organic precursors for functional oxide preparation: Thin films versus powders, Thermochim. Acta. 601 (2015) 1–8. doi:10.1016/j.tca.2014.12.016.